4.2.3.6 Planetary photometry and spectroscopy

KATRIN STEPHAN

4.2.3.6.1 Photometric properties of planetary surfaces

Photometry is one of the basic remote sensing techniques of astronomy and planetary science. Visual photometry allows the detection of a rotational light curve, to establish whether or not the rotation is in resonance with the orbital period of astronomical objects. It also allows investigation of the photometric phase curve, which contains albedo information [79Bow] and also yields an absolute *V* magnitude at unit distance to Earth and Sun, which allows a determination of the diameter if the albedo is known [80Deg] (Tables 1 - 3).

The most widely used photometric system, the UBV-system or Johnson-Morgan system is a broad band photometric system for the classification of planetary objects according to their colors [53Joh]. The letters U, B, and V stand for 'ultraviolet', 'blue' and 'visual magnitudes' that represent color filters which are sensitive at 364, 442, and 540 nm, respectively.

Little compositional information can be obtained from UBV-colors alone but it is usually possible to recognize principal compositional types identified by more sophisticated techniques like spectroscopy (see Section 4.2.3.6.2) and to select exceptional objects for further studies [76Zel, 78Bow, 79Zel].

More recently, photometric observations of planetary objects are compared to photometric models that incorporate specific physical parameters of their surfaces [88Bur]. The agreement or lack of agreement between the observation and the model helps to constrain the model parameters and leads to a more accurate characterization of the body. The most recent photometric model has been developed by [81Hap] and can be written in the form:

$$I(\mu_0,\mu,\alpha) = F\frac{\varpi_0}{4}\frac{\mu_0}{+\mu_0}\left[S(\alpha,h)P(\alpha,g) + H(\mu)H(\mu_0) - 1\right] \quad (1)$$

where I is the bidirectional reflectance of the planetary object observed at a specific incidence (μ_0), emission (μ) and phase angle α, F is the incident solar flux, ω_0 the single scattering particle albedo, $S(\alpha,h)$ the shadowing function, and $P(\alpha,g)$ the single particle scattering function that can be approximated by a Henyey-Greenstein phase function:

$$P(\alpha,g) = \frac{1-g^2}{(1+g^2+2g\cos\alpha)^{3/2}} \quad (-1 < g < +1) \quad (2)$$

where g is the asymmetry parameter (cos α). The parameter h is called the compaction parameter and is related to the porosity of the surface [81Hap]. Hapke parameters derived for planetary satellites are summarized in Table 4.

Table 3. Hemispheric disk-integrated photometric properties of small planetary satellites adapted [93Ast], [06She], c - [06Jac], d - [06Nic]; : Quantity is uncertain. See Table 1 for explanation of symbols.

	Satellite		V_0	$V_{(1,0)}$	p_v
Jupiter	J5	Amalthea	+14.1	+7.4	0.09 (c)
	J6	Himalia	+14.6 (d)	+8.14	0.03 (c)
	J7	Elara	+16.3 (b)	+10.0 (b)	0.03 (c)
	J8	Pasiphae	+17.03	+10.33	~0.04 (c)
	J9	Sinope	+18.1 (d)	+11.6	~0.04 (c)
	J10	Lysithea	+18.3 (d)	+11.7 (b)	~0.04 (c)
	J11	Carme	+17.6 (d)	+11.3 (b)	~0.04 (c)
	J12	Ananke	+18.8 (d)	+12.2 (b)	~0.04 (c)
	J13	Leda	+19.5 (d)	+13.5	~0.04 (c)
	J14	Thebe	+16.0 (d)	+9.0	0.047 (c)

	Satellite		V_0	$V_{(1,0)}$	p_v
	J15	Adrastea	+18.7 (d)	+12.4	0.05 (c)
	J16	Metis	+17.5	+10.8	0.061 (c)
	J17	Callirrhoe	+20.7 (d)	+14.2 (b)	0.06 (d)
	J18	Themisto	+21.0 (d)	+14.4 (b)	0.06 (d)
	J19	Megaclite	+21.7 (d)	+15.0 (b)	0.06 (d)
	J20	Taygete	+21.9 (d)	+15.4 (b)	0.06 (d)
	J21	Chaldene	+22.5 (d)	+15.7 (b)	0.06 (d)
	J22	Harpalyke	+22.2 (d)	+15.7 (b)	0.06 (d)
	J23	Kalyke	+21.8 (d)	+15.3 (b)	0.06 (d)
	J24	Iocaste	+21.8 (d)	+14.5 (d)	0.06 (d)
	J25	Erinome	+22.8 (d)	+16.0 (b)	0.06 (d)
	J26	Isonoe	+22.5 (d)	+15.9 (b)	0.06 (d)
	J27	Praxidike	+21.2 (d)	+15.0 (b)	0.06 (d)
	J28	Autonoe	+22.0 (d)	+15.4 (b)	0.06 (d)
	J29	Tyone	+22.3 (d)	+15.7 (b)	0.06 (d)
	J30	Hermippe	+22.1 (d)	+15.5 (b)	0.06 (d)
	J31	Aitne	+22.7 (d)	+16.1 (b)	0.06 (d)
	J32	Eurydome	+22.7 (d)	+16.1 (b)	0.06 (d)
	J33	Euanthe	+22.8 (d)	+16.2 (b)	0.06 (d)
	J34	Euporie	+23.1 (d)	+16.5 (b)	0.06 (d)
	J35	Orthosie	+23.1 (d)	+16.5 (b)	0.06 (d)
	J36	Sponde	+23.0 (d)	+16.4 (b)	0.06 (d)
	J37	Kale	+23.0 (d)	+16.4 (b)	0.06 (d)
	J38	Pasithee	+23.2 (d)	+16.6 (b)	0.06 (d)
	J39	Hegemone	+22.8 (d)	+15.9 (b)	0.04 (d)
	J40	Mneme	+23.3 (d)	+16.3 (b)	0.04 (d)
	J41	Aoede	+22.5 (d)	+15.8 (b)	0.04 (d)
	J42	Thelxinoe	+23.4 (d)	+16.4 (b)	0.04 (d)
	J43	Arche	+22.8 (d)	+16.4 (b)	0.04 (d)
	J44	Kallichore	+23.7 (d)	+16.8 (b)	0.04 (d)
	J45	Helike	+22.6 (d)	+16.0 (b)	0.04 (d)
	J46	Carpo	+23.0 (d)	+15.6 (b)	0.04 (d)
	J47	Eukelade	+22.6 (d)	+15.0 (b)	0.04 (d)
	J48	Cyllene	+23.2 (d)	+16.2 (b)	0.04 (d)
Saturn	S10	Janus	+14.4 (d)	+ 4.4 :	0.6 (c)
	S11	Epimetheus	+15.6 (d)	+ 5.4 :	0.5 (c)
	S12	Helene	+18.4 (d)	+ 8.4 :	0.6 (c)
	S13	Telesto	+18.5 :	+ 8.9 :	0.7 : (d)
	S14	Calypso	+18.7 :	+ 9.1 :	1.0 (c)
	S15	Atlas	+19.0 (d)	+ 8.4 :	0.4 (c)
	S16	Prometheus	+15.8 (d)	+ 6.4 :	0.6 (c)
	S17	Pandora	+16.4 (d)	+ 6.4 :	0.5 (c)
	S18	Pan	+19.4 (d)		0.5 :
	S19	Ymir	+21.6 (d)		0.06 :(c)
	S20	Paaliag	+21.2 (d)	+12.2	0.06 :(d)
	S21	Tarvos	+22.0 (d)	+13.2	0.06 :(d)
	S22	Ijiraq	+22.5 (d)	+13.6	0.06 :(d)
	S23	Suttungr	+23.8 (d)		0.06 :(c)
	S24	Kiviuq	+21.9 (d)	+13.1	0.06 :(d)
	S25	Mundilfari	+23.7 (d)	+14.8	0.06 :(d)
	S26	Albiorix	+20.4 (d)		0.06 :(c)
	S27	Skadi	+23.5 (d)	+14.8	0.06 :(d)
	S28	Erriapo	+22.9 (d)	+14.0	0.06 :(d)
	S29	Siarnaq	+20.0 (d)		0.06 :(c)
	S30	Thrymr	+23.8 (d)	+14.8	0.06 :(d)
	S31	Narvi	+24.1 (d)		0.06 :(d)
	S32	Methone	+25.1 (d)		
	S33	Pallene	+24.5 (d)		

	Satellite		V_0	$V_{(1,0)}$	p_v
	S34	Polydeuces	+24.8 (d)		
	S35	Daphnis			
Uranus	U6	Cordelia	+24.2 (d)	+11.4	0.07 :(d)
	U7	Ophelia	+23.9 (d)	+11.1	0.07 :(d)
	U8	Bianca	+23.1 (d)	+10.3	0.07 :(d)
	U9	Cressida	+22.3 (d)	+ 9.5	0.07 :(d)
	U10	Desdemona	+22.5 (d)	+ 9.8	0.07 :(d)
	U11	Juliet	+21.7 (d)	+ 8.8	0.07 :(d)
	U12	Portia	+21.1 (d)	+ 8.3	0.07 :(d)
	U13	Rosalind	+22.5 (d)	+ 9.8	0.07 :(d)
	U14	Belinda	+22.1 (d)	+ 9.4	0.07 :(d)
	U15	Puck	+20.4 (d)	+ 7.5	0.07 :(d)
	U16	Caliban	+22.4 (d)	+ 9.7	0.07 :(d)
	U17	Sycorax	+20.8 (d)	+ 8.2	0.07 :(d)
	U18	Prospero	+23.2 (d)	+11.0	0.07 :(d)
	U19	Setebos	+23.3 (d)	+11.1	0.07 :(d)
	U20	Stephano	+24.1 (d)	+11.9	0.07 :(d)
	U21	Trinculo	+25.3 (d)		0.06 :(d)
Neptune	N3	Naiad	+24.6 (d)	+10.0 :	0.06 :(d)
	N4	Thalassa	+23.9 (d)	+ 9.1 :	0.06 :(d)
	N5	Despina	+22.5 (d)	+ 7.9	0.06 (c)
	N6	Galatea	+22.4 (d)	+ 7.6 :	0.06 :(c)
	N7	Larissa	+22.0	+ 7.3	0.06 (c)
	N8	Proteus	+20.3	+ 5.6	0.06 (c)

Table 1. Photometric properties of the terrestrial planets in the UBV system from [76Ast], [93Ast], (a) [88Vev], (b) [94Kar].

V_0 mean opposition magnitude of the satellite

$V_{(1,0)}$ absolute visual magnitude reduced to a phase angle of zero (α = 0°) and planet-Sun distances of 1 Astronomical unit

B-V / U-B Color index of Voyager-Filters

p_v geometric visual albedo of a planetary object - ratio of its actual brightness at zero phase angle (i.e. as seen from the light source) to that of an idealized flat, fully reflecting, diffusively scattering (Lambertian) disk with the same cross-section.

q phase integral given in terms of the directional scattered flux $I(\alpha)$ into phase angle α (averaged over all wavelengths and azimuthal angles) as:

$$q = 2\int_0^{\pi} \frac{I(\alpha)}{I(0)} \sin\alpha \, d\alpha$$

A_B Bond Albedo - related to the geometric albedo p_v by $A = pq$

			Color index				
	V_0	$V_{(1,0)}$	*B-V*	*U-B*	p_v	q	A_B
Mercury	–0.21 (a)	–0.42 (a)	–0.91	–0.4	0.096	0.58	0.056
					0.138 (a)	0.486 (a)	0.119 (a)
Venus	–3.81	–4.34	0.79	0.5	0.6	1.2	0.72
Earth	–3.87	–3.9	0.2	?	0.37	1.05	0.39
Mars	–2.01	–1.51	1.37	0.6	0.154	1.02	0.16
			1.49 (b)				

Table 2. Hemispheric disk-integrated photometric properties of large planetary satellites adapted from [93Ast], [06She], c - [06Jac], d - [06Nic], e - [73Lan], f - [86Han], g – [88Bur], h - [91Bur], i - [93Hil], (8) Bright side, 0.5; faint side, 0.05. For explanation of symbols see Table 1.

	Satellite				Color index				
			V_0	$V_{(1,0)}$	*B-V*	*U-B*	p_v	q	A_B
Earth		Moon	−12.74	+0.21	0.92	0.46	0.12	0.611 (e)	0.123 ± 0.002 (e)
Mars	M1	Phobos	+11.4 (d)		0.65	0.18	0.07	0.27	0.02
	M2	Deimos	+12.5 (d)	+12.89	0.65	0.18	0.068 (c)	0.32	0.02
Jupiter	J1	Io	+5.02	−1.68	1.17	1.30	0.62		
	J2	Europa	+5.29	−1.41	0.87	0.52	0.68 0.78 ± 0.03 (g)	1.09 ± 0.11 (g)	0.62 ± 0.14 (g)
	J3	Ganymede	+4.61	−2.09	0.83	0.50	0.44 (c)	0.78 ± 0.06 (h)	0.35 ± 0.03 (h)
	J4	Callisto	+5.6 (d)	−1.05	0.86	0.55	0.19 (c)	0.51 ± 0.06 (h)	0.11 ± 0.02 (h)
Saturn	S1	Mimas	+12.8 (d)	+3.3			0.6 (c)		
	S2	Enceladus	+11.8 (d)	+2.1	0.7	0.28	1.0		1.4
	S3	Tethys	+10.3 (d)	+0.6	0.73	0.30	0.8 (c)		
	S4	Dione	+10.4	+0.8	0.71	0.31	0.6 (c)		
	S5	Rhea	+9.7	+0.1	0.78	0.38	0.6 (c)		
	S6	Titan	+8.4 (d)	−1.28	1.28	0.75	0.2 (c)		
	S7	Hyperion	+14.4 (d)	+4.63	0.78	0.33	0.3		
	S8	Iapetus	+11.0 (d) (10.2 - 11.9 (f)	+1.5	0.72	0.30	0.2 (8)		
	S9	Phoebe	+16.5 (d)	+6.89	0.70	0.34	0.081 (c)		
Uranus	U1	Ariel	+13.7 (d)	+ 1.45			0.39 (c)	0.65	0.31 ± 0.06 (f)
	U2	Umbriel	+14.5 (d)	+ 2.10			0.21 (c)	0.68	
	U3	Titania	+13.5 (d)	+ 1.02			0.27 (c)	0.70	
	U4	Oberon	+13.7 (d)	+ 1.23			0.23 (c)	0.68	
	U5	Miranda	+15.8 (d)	+ 3.6			0.32 (c)		0.24 ± 0.06 (f)
Neptune	N1	Triton	+13.5 (d)	−1.24			0.756 (c)	0.72 1.17 ± 0.03 (i)	0.29
	N2	Nereid	+19.7 (d)	+ 4.0			0.155 (c)	0.65	

Table 4. Hapke parameters of terrestrial planets and satellites from (a) [04Pap] and references therein, (b) [86Vev], (c) [98Sim], (d) [87Hel], (e) [95Bur], [91Bur], (f) [97Dom], (g) [91Dom], (h) [86Sim], (i) [85Bur], (j) [88Bur], (k) [89Ver], (l) [88Hel], (m) [90Bur1], (n) [90Hil], (o) [88Vev]. Mercury two solutions: 1. was obtained by fitting the phase curve on a linear I/F scale – 2. involved fitting the near opposition portion ($\leq$ 20°) on a linear scale and the remainder on a magnitude scale.

ω_0 single scattering particle albedo
S_0 shadowing function or strength of the opposition surge (phase angle =0)
P_0 single particle scattering function (phase angle = 0)
h width of the opposition surge or compaction parameter,
θ effective surface tilt, also called the macroscopic roughness angle
Void space % $1 - \rho/\rho_0$

Planet	Satellite			ω_0	P_0	θ [°]	h	Void space [%]	References
Mercury				0.2 / 0.21		21/25	0.11/0.09	90	d, i, o
Earth		Moon	(0.56µm)	0.28		26	0.07		a, d, i
			(0.47µm)	0.21	−0.25±0.02	20	0.4 ± 0.1		
Mars	M1	Phobos		0.0549	−0.13	21	0.072	87	c, h, j
Jupiter	J1	Io		0.87	−0.2	25		65	h, i, k
	J2	Europa (0.47µm)	Global	0.97	−0.15 ± 0.04	23	1.0 ± 0.2		a, d, i, k
			Leading side	0.92		10			g
			Trailing side	0.90		10		80	e, g
	J3	Ganymede (0.47µm)	Global	0.76 ± 0.01	−0.2±0.04	28 ± 1			a, e
				0.80 ± 0.4		29 ± 4			
			Dark terrain	0.607 ± 0.005		25.1 ± 0.1	0.32 ± 0.007	80	e
			Bright terrain	0.612 ± 0.005		2.7 ± 0.1	0.10 ± 0.01		
			Leading side	0.82 ± 0.03	−0.20±0.04			80	e, f, g
				0.83 ± 0.01					
			Trailing side	0.78 ± 0.03	−0.21±0.04			90	f, g
				0.87 ± 0.01					
	J4	Callisto	Global	0.44 ± 0.03	−0.35 ± 0.05	32 ± 3		92	e
			Leading side	0.43 ± 0.03	−0.23±0.02	36 ± 3		88	e
			Trailing side	0.45 ± 0.03	−0.17 ± 0.02	29 ± 3		80	e, i
Saturn	S1	Mimas		0.93 ± 0.03	−0.30 ± 0.05	30	0.7 ± 0.2		d, i
	S2	Enceladus		0.99 ± 0.02	−0.35 ± 0.03		0.4 ±0.2	90	i, k
	S5	Rhea		0.76 ± 0.03	−0.35 ± 0.05	16 ± 3	0.4 ± 0.1	92	i, k, l

Planet	Satellite		ω_0	P_0	θ [°]	h	Void space [%]	References
Uranus	U5	Miranda	0.55	–0.31	32 ± 9		92	l, m
	U1	Ariel	0.58 ± 0.05	–0.28 ± 0.05	28 ± 3		75	l, m
	U2	Umbriel	0.25 ± 0.03	–0.25 ± 0.03	18 ± 3		92	l, m
	U3	Titania	0.50 ± 0.02	–0.20 ± 0.03	25 ± 5		92	l, m
	U4	Oberon	0.35 ± 0.05	–0.20 ± 0.03	20 ± 3			l, m
Neptune	N1	Triton	0.994 ± 0.004	–0.28±0.03	10 ± 2			n

Table 5. Summary of satellites radar properties derived from earth-based (Arecibo 13-cm observation and Goldstone 3.5-cm observations and spacecraft measurements [07Bus], [92Ost], [77Cam], [78Cam], [01Bla], [07Bla], [06Ost], [07Wye], [90Muh].

OC radar albedo measured in the opposite polarization
SC radar albedo measured in the same circular polarization
OL radar albedo measured in the orthogonal linear polarization
SL radar albedo measured in the same linear polarization
TP total power albedo (*TP* = *SL*+ *OL* = *SC*+ *OC*)
μC Circular polarization ratio (*SC*/*OC*)
μL Linear polarization ratio (*OL*/*SL*)

Planet		Satellite	Wavelength	*TP*	*OC*	*SC*	*OL*	*SL*	*n*	References
Mars	M1	Phobos			0.064±0.014					07Bus
					0.056±0.014					
	M2	Deimos			0.021±0.006					07Bus
Jupiter	J2	Europa	3.5-cm	2.31±0.36	0.91±0.13	1.40±0.23				92Ost, 06Ost
			13-cm	2.60±0.22	1.03±0.08	1.58±0.14	0.83±0.21	1.77±0.44	1.73±0.08	92Ost, 77Cam, 78Cam, 06Ost
			70-cm	<0.95±0.36	<0.17	<0.17				01Bla, 06Ost
	J3	Ganymede	3.5-cm	1.55±0.20	0.65±0.10	0.90±0.10				92Ost, 06Ost
			13-cm	1.39±0.14	0.57±0.06	0.82±0.09	0.48±0.11	1.03±0.24	1.46±0.04	92Ost, 77Cam, 78Cam, 06Ost
			70-cm	0.62±~0.2	0.25±0.09	0.37±0.11				01Bla, 06Ost
	J4	Callisto	3.5-cm	0.72±0.06	0.32±0.02	0.40±0.04				92Ost, 06Ost
			13-cm	0.69±0.06	0.32±0.03	0.37±0.03	0.23±0.06	0.41±0.11	1.43±0.05	92Ost, 77Cam, 78Cam, 06Ost
			70-cm	≤0.18±0.06	<0.02	0.15±0.06				01Bla, 06Ost

Planet	Satellite	Wavelength	*TP*	*OC*	*SC*	*OL*	*SL*	*n*	References
S2	Enceladus (Avg.)	2.2-cm					1.60	12.0±0.9	06Ost
	Enceladus (Avg.)	13-cm	1.94±0.31	1.07±0.22	0.86±0.20			12.0±0.9	07Bla
	Enceladus (L)	13-cm	2.55±0.42	1.16±0.29	1.39±0.29				07Bla
	Enceladus (T)	13-cm	0.78±0.28	1.00±0.28	≤0.54				07Bla
S3	Tethys						1.54	1.8±0.8	06Ost
	Tethys	13-cm	1.45±0.13	0.66±0.09	0.79±0.09				07Bla
S4	Dione	2.2-cm					0.94	1.6±0.7	06Ost
	Dione	13-cm	0.74±0.10	0.41±0.07	0.32±0.07				07Bla
S5	Rhea						1.06	1.7±0.8	06Ost
	Rhea	13-cm	1.31±0.05	0.61±0.03	0.71±0.04				07Bla
S6	Titan	2.2-cm	<0.4	0.34					07Wye
		13-cm	0.21						90Muh, 07Wye
S8	Iapetus (L)	2.2-cm					0.31	1.1±0.1	06Ost
	Iapetus (T)	2.2-cm					0.57	1.3±0.6	06Ost
S9	Phoebe	2.2-cm					0.18	0.9±0.2	06Ost

4.2.3.6.2 Spectral properties of planetary surfaces

Most of our information concerning the elemental and mineralogical composition of the planetary surfaces and physical state of the constituents is derived from spectral measurements. Individual atomic and molecular species possess unique and identifiable spectral signatures with their frequency (wavenumber or wavelength) defined by the quantum structure of specific atoms and molecules. Characteristic spectral features are to be found especially in the microwave, infrared, visible and ultraviolet regions, and they are caused by a variety of transition types within atoms and/or molecules e.g. rotations, vibrations, or electronic transitions, respectively.

4.2.3.6.2.1 Radar observations

A Radar (Radio Detection and Ranging) system detects distant objects by emitting radio or micro waves and analyzes the returned "echos" reflected by the target. The delay between emitting and receiving the returning signal enables to determine the distance between the instrument and the target. The direction of the beam determines the direction of the reflection. The polarization and frequency of the return can sense characteristics of planetary surfaces deeper than apparent to visible imaging. Common transmissions of a circular polarized signal and reception of echoes in the same circular (*SC*) and opposite (*OC*) polarizations are used (i.e. earth-based Arecibo 13-cm- and Goldstone 3.5-cm-observations). In rare cases the transmission is linearly polarized, with reception in the same linear (*SL*) and orthogonal linear (*OL*) polarizations (i.e. Radar instrument onboard the Cassini spacecraft).

Terrestrial planets and satellites
Radar echos from terrestrial planets and satellites like the Moon are dominated by quasi-specular scattering properties, which means they are characterized by low radar albedos i.e. ~ 0.1 at 3.5 and 13 cm (Fig. 1), and most of the echo power has the rotational sense opposite to that transmitted (expressed by a relatively low circular polarization ratio μC (*SC/OC*) of ~ 0.1 - 0.3). A perfectly smooth surface would have a polarization ratio of zero, but moderate surface variations cause some echo power in the other polarization sense. To give an example, anomalous bright radar features are consistent with water ice deposits at the poles of Mercury [93But, 92Har1], and fresh volcanic lava flows on Mars are very rough at dm-scales [92Har2]; although for most surfaces the total albedo still remain low (Table 5).

Outer planets satellites
In contrast icy satellites scatter radar energy like very rough surfaces do, indicated by their unusual high radar albedos (Fig. 1, Table 5) as well as very high circular polarization ratios (~1.5) compared to terrestrial planets [92Ost]. Similarly, linear polarization measurements also show significant power in the unexpected polarization. Their polarization ratios μL (the polarization ratio is defined as the ratio of power in the sense orthogonal to the transmitted (*OL*) to the power in the parallel (or same) sense (*SL*)) fall around 0.5. Although most of the radar echo of the Saturnian satellite Titan is also characterized by a diffusely scattered component, a small specular component is consistent with those expected for areas of liquid hydrocarbons [03Cam].

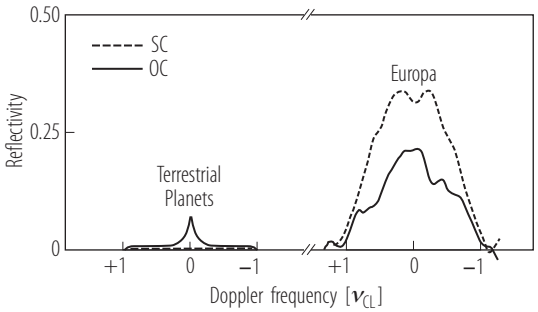

Fig. 1. Radar spectra of terrestrial and icy Solar System bodies [82Ost].

4.2.3.6.2.2 Thermal infrared spectroscopy

The IR spectrum of a planetary surface can include both absorption and emission bands diagnostic of the surface composition that complement the results derived from VIS-NIR spectroscopy (see Section 4.2.3.6.2.3). Various anionic groups (e.g., SiO_4, CO_3, SO_4, etc.) exhibit internal and lattice vibrational fundamental modes within this wavelength range that are at least one order of magnitude more intense than any associated combinations and/or overtones at wavelengths less than 5 μm. In addition they are extremely sensitive to minor concentrations of these absorbing species. Especially the strong fundamental vibrational reststrahlen bands of Si-O located in the wavelength range from 7 to 12 μm make this region sensitive to all silicates, whereas only Fe-bearing minerals can be detected from electronic bands in shorter wavelength (0.8 - 2.5μm) reflectance spectra [06War]. Specific energies (wavelength position) and relative intensities of these vibrational modes can be used to distinguish between icy vs. rocky surfaces, different chemical groups (e.g. carbonates vs. silicates), different structural groups with similar compositions (sorosilicates vs. phyllosilicates), differing chemical variations within a group ($CaCO_3$ vs. $FeCO_3$), and differing structural polymorphs of the same compound (e.g. calcite vs. aragonite).

Terrestrial planets and satellites

Thermal IR spectra suggest a significant difference in the compositional and/or structural properties of Mercury and the Moon. According to observed emittance spectral features, there is strong evidence of the presence of Fe-poor pyroxenes and intermediate feldspars on Mercury, heterogeneously distributed across the surface on regional scales [98Spr, 02Spr].

Data from the recent Mars missions show that the mafic regions have much more diversity than previously recognized [05Chr]. Significant concentrations (> 0.10) of plagioclase and high-Ca pyroxene, sheet silicates/high-Si glass, and hematite are detected [02Ban, 05Yen]. Elevated concentrations of plagioclase and high-Ca pyroxene correspond to basaltic surfaces located in low albedo highlands regions north of ~ 45°S. Significant concentrations of plagioclase and sheet silicates/high-Si glass and low concentrations of high-Ca pyroxenes are consistent with andesitic surfaces and are concentrated in both southern and northern high-latitude, low-albedo regions [02Ban, 05Yen]. Other emissions and absorption features in the 5.4 and 10.5 μm wavelength region have been associated with sulphates, carbonates, and hydrates [90Pol]. Observations in the thermal infrared have demonstrated that CO_2 ice is the major component of the seasonal caps of Mars [71Neu, 79Kie, 00Kie]. During northern spring a moderately cold and bright ring lagging a few degrees of latitude behind the receding boundary of regions at CO_2 sublimation temperatures (160 - 170 K) has been observed and interpreted as H_2O frost [01Kie] and confirmed by observations in the near infrared [05Bib, 07Lan] (see Section 4.2.3.6.2.4).

Outer planet satellites

The volcanic component on Io's surface accounts for the increase in brightness temperature at shorter wavelengths. Broad shallow features in the 10 - 30 μm spectral regions may come from surface SO_3 [95Kha, 99Spe, 89Nas]. In contrast, the emission spectra from the other icy satellites in the outer Solar System are mostly featureless, nearly black body emission spectra (Fig. 3).

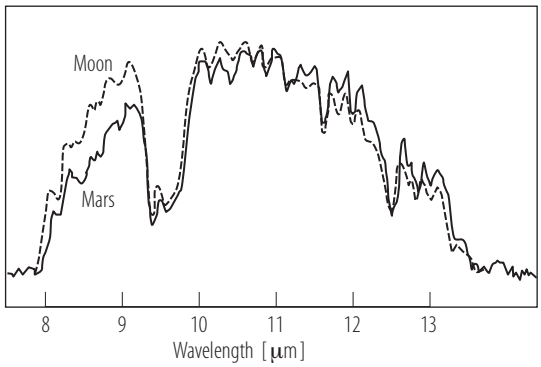

Fig. 2. The infrared spectrum of the Moon (dashed line) and Mars (solid line) obtained with a grating spectrometer attached to the 5.08-m telescope at Mount Palomar [60Sin].

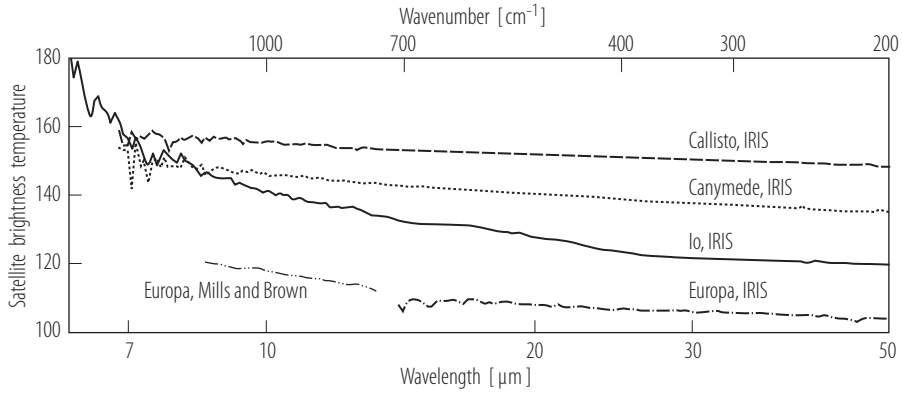

Fig. 3. Emission spectra of the Galilean satellites obtained by the Voyager Infrared Interferometer Spectrometer (IRIS) [87Spe] and a ground-based Europa spectrum scaled to the spectrum of Callisto (8.5 - 13.3 μm) from [00Mil]. The fine structures at shorter wavelengths are probably noise [04Spe].

4.2.3.6.2.3 Radiometry

In contrast to the visible and near-infrared spectral region, where planets and satellites reflect solar radiation, thermal emission becomes an increasingly dominant source of the energy sampled by remote sensing observations at longer wavelengths. Thermally emitted photons from a planetary surface can be used to deduce the surface thermal properties. Monochromatic fluxes at one or two wavelengths can be used to derive model dependent surface temperatures, while measurements at many wavelengths allow detailed thermal modelling (Table 6 + 7).

Thermal observations combined with visual observations can be used to derive the albedo of the surface [82Bro] which can help to constrain the surface composition. Measurements obtained as a function of time as the surface passes into the night side, or through an eclipse, can be used to derive thermal conductivity [77Mor]. The thermal conductivity depends on the microstructure as well as the surface material, and thus provides another constraint on surface composition.

Table 6. Global surface temperatures of terrestrial planets and satellites

T_{disk} average 2-cm or 6-cm brightness temperature measured over a disk of the assumed radius of the satellite

T_{eq} isothermal equilibrium temperature was calculated using the Bond albedo A_{Bond} ($T_{eq} = 91.4\ (1 - A_{Bond})^{1/4}$ (see Section 4.2.3.6.1)

E emissivity is equal to T_{disk} / T_{eq}

Planet	Satellite	T_{disk} [K]	T_{min} [K]	T_{max} [K]	References
Mercury		452	100	700	75Str
Venus		~ 735			79Sei
Earth		281	260 - 283	310	99Har
	Moon	220 (eq)	100	390	99Vas
Mars		227	186	268	
		215	150	275	07Lan
Jupiter	Io	106		130	99Har
	Europa	97	86	132	99Spe, 96Ort
	Ganymede	107	90	152	99Spe, 96Ort
	Callisto	134 ± 11	80 ± 5	165 ± 5	87Spe, 04Moo
Saturn	Phoebe		82	112	05Fla
	Tethys	93 ± 4			82Han
	Enceladus	75 ± 3			82Han
		75	32.9	145	06Spe
	Titan	93.7			07Mit
Uranus	Ariel	84 ± 1			86Han
	Miranda	86 ± 1			86Han
Neptun	Triton	38			89Con

Table 7. Radiometric results of the Galilean and Saturnian satellites are from [84deP] and [06Ost], respectively. Please see Table 6 for explanation of symbols.

Satellite		T_{disk} [K]	T_{eq} [K]	E
Europa	2-cm	47 ± 10	97	0.48
	6-cm	44 ± 10	97	0.45
Ganymede	2-cm	67 ± 6	107	0.63
	6-cm	55 ± 6	107	0.51
Callisto	2-cm	92 ± 9	117	0.79
	6-cm	105 ± 7	117	0.90
Enceladus	2-cm	33.4	56.9	0.59
Iapetus (L)	2-cm	73.0	89.9	0.81
Iapetus (T)	2-cm	57.1	83.3	0.69
Phoebe	2-cm	84.1	91.3	0.92
Rhea	2-cm	45.5	78.7	0.59
Tethys	2-cm	32.0	72.7	0.44
Dione	2-cm	50.8	78.7	0.65

4.2.3.6.2.4 From near infrared to UV

Spectroscopy in the spectral range from UV to NIR is the major tool in the study of the mineral composition and physical state of the constituents of planetary surfaces. UV, visible, and NIR reflectance spectroscopy (UVVNIR) is a well established technique, with the first NIR spectra obtained in the laboratory by Sir William Herschel over 190 years ago. This technique is based on the analysis of reflected electromagnetic radiation from a sunlit Solar System object as a function of viewing geometry and wavelength, and the comparison of the acquired spectrum with reference reflectance spectra of samples measured in laboratories. Spectra in this wavelength region are particularly well suited to remote sensing studies because of the variety of mechanisms that can produce photon absorptions. These mechanisms include electronic transitions in molecular orbitals and vibrational transitions in molecules and crystals, as well as electronic transitions within and between atoms (crystal field, metal-metal intervalence charge transfer, and oxygen-metal charge transfer) [93Bur, 80Hun, 93Sal]. In addition, UVVNIR spectra are largely free of thermal emission features, which affect mid infrared spectra (see Section 4.2.3.6.2.2). The precise wavelength range available for reflectance studies of planetary surfaces varies with temperature, and therefore with location in the Solar System. For example, on Mercury thermally emitted radiation begins at 1.6 μm [88Vil], while pure reflectance spectra for icy bodies in the outer Solar System may be obtained out to 4 - 5 μm without interference from thermal emission.

The terrestrial planets and the Moon

Silicates (e.g. pyroxene, olivine, feldspar, phyllosilicates) are ubiquitous on Earth and throughout the inner Solar System (i.e. on Mars, Fig. 4). They exhibit diagnostic Fe^{2+} electronic transition absorption bands in the visible and near infrared spectral region [75Ada]. One exception is Mercury. Spectra show an extremely low probability of the Fe^{2+} charge-transfer absorption band in reflected light from Mercury's surface indicating that FeO in the regolith is very low in abundance, if present at all [86Vil, 97Ble, 02War]). This is also supported by results derived from IR spectroscopy [98Spr, 02Spr] (see Section 4.2.3.6.2.2).

Similar to Mercury the spectra of lunar minerals are generally simpler than Earth spectra since they contain no additional features due to Fe^{3+} or OH^-. Lunar pyroxenes exhibit two diagnostic Fe^{2+} electronic transition absorption bands, one centered near 1 μm, the other near 2 μm. The actual position of the band centers move to longer wavelength as Ca and Fe substitute for Mg in the pyroxene structure [75Ada]. Lunar Maria basalt contain abundant high-Ca pyroxene (> 50%) that is indicative of their basaltic nature. When olivine is also present in significant amounts (10 - 20%), its effect is to broaden the pyroxene absorption at 1 μm and move the center to slightly longer wavelengths. In contrast, lunar highland rocks contain various amounts of feldspar and different types of mafic minerals.

Ilmenite ($FeTiO_3$) is the most abundant oxide mineral found in lunar rocks, varying from 0 to 24 vol% [82Pa] and exhibits broad absorptions near 0.5 and 1.2 μm ([75Ada, 93Bur]). The Ilmenite content in mare basalt is normally detected only indirectly by the amount of Fe and Ti incorporated into the lunar regolith (see Section 4.2.3.6.2.5).

Glass, although technically not a mineral, is of geological importance on the Moon, both as a product of space weathering and in pyroclastic deposits, characterized by broad features at 1 and 2 μm due to ferrous iron [85Gad, 03Gad].

Hydrated materials like phyllosilicates and sulfates are common on Earth and were also identified on Mars [05Bib, 05Pou, 05Gen] (Fig. 4). Carbonate rocks comprise one-fifth to one-fourth of the terrestrial stratigraphic record. Based on IR spectra carbonates are supposed to be found on Mars (see Section 4.2.3.6.2.2), but have not been identified in the NIR spectral range yet [05Bib].

Ices and frosts are not only abundant on Earth but also existent on Mars with a water-ice composition of the north polar perennial cap, and a thin CO_2-ice veneer for the south cap [05Bib] (Table 8).

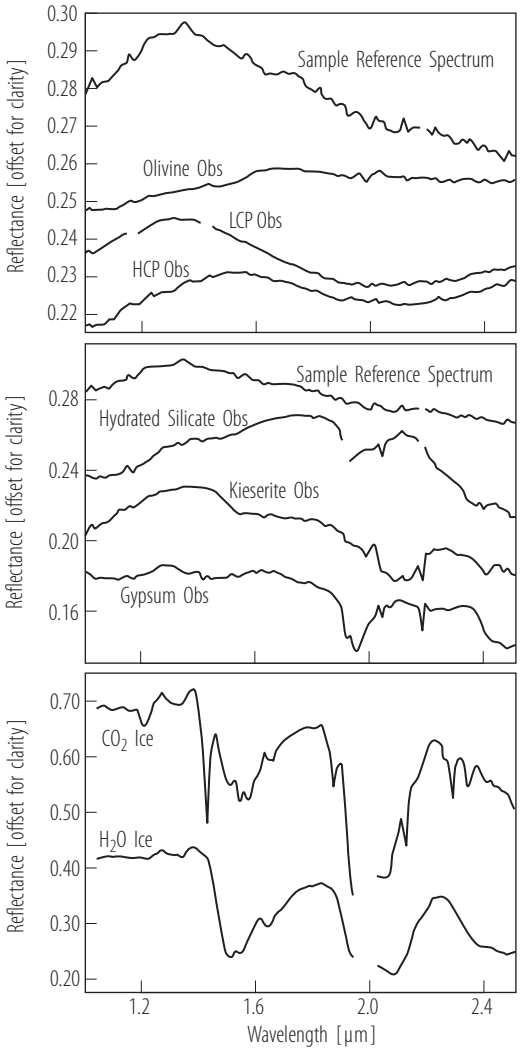

Fig. 4. Representative spectra representing the mineralogic diversity that has been detected on the surface of Mars derived from the Mars Express OMEGA experiment. These example spectra show spectral signatures dominated by a specific mineral species: **(a)** olivine and high-(HCP) and low-calcium pyroxenes; **(b)** hydrated silicates, sulfates like kieserite and gypsum and **(c)** ices like water and CO_2 ice [07Pel].

Outer planets satellites

Despite the progress in data collection since the era of the Voyager missions, SO_2 (frozen and gaseous) is still the only compound that definitely has been identified on Io's surface and its spectral features dominate the Io spectra from UV up to the Near Infrared (Fig. 5).

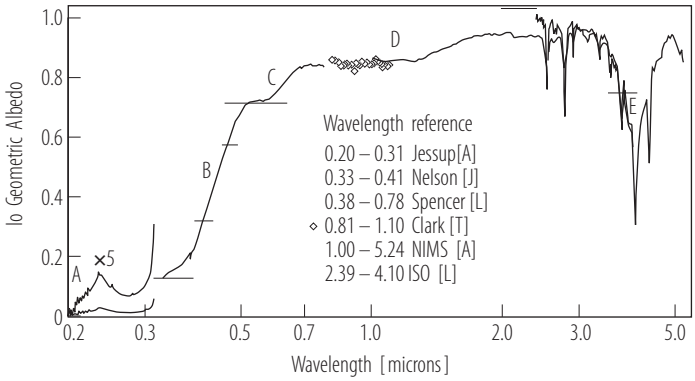

Fig. 5. Io reflectance spectrum: Spectral identifications: A = SO_2 gas (fine structure below 0.23 μm); B = S_8 or SnO; C = S_4; D = unkown; E = Cl_2SO_2 (?). Other features are due to SO_2 frost. (L = leading hemisphere; T = trailing hemisphere; J = Jupiter facing hemisphere; A = Anti Jovian hemisphere) ([95Spe], [86Cla], NIMS: [97Car], ISO: [04Spe]).

Galileo NIMS results show that frozen SO_2 exists almost everywhere on the surface. Regions with abundant SO_2 are related to plumes that are located close to the equator [97Car]. The only regions lacking SO_2 are situated in the vicinity of hot spots, where surface temperatures are sufficiently high enough to vaporize or prevent the condensation of SO_2 [01Dou]. In addition, elemental sulfur is thought to be common on Io's surface [98Nas] absorbing in the UV and blue light but is highly reflective and featureless in the near-IR [82Fan]. The variety of surface colors and spectral shapes at ultraviolet-visible wavelength match several sulfur allotropes [91Mos] (Fig. 5). Additional spectral features were observed in the UV and NIR that cannot be attributed to SO_2 but possibly indicate SO_3 [86Nel] and H_2O and H_2S frozen in SO_2 [90Sal], Cl_2SO_2 [03Sch], as well as hydrated or hydrogen bearing species [97Car] on Io's surface [04Spe].

Spectroscopic observations have shown the clear presence of H_2O ice on the surfaces of the Galilean satellites Europa, Ganymede, and Callisto (Fig. 6), on at least eight relatively large satellites (excluding Titan) and the rings of Saturn, as well as the five largest satellites of Uranus (Miranda, Ariel, Umbriel, Titania, and Oberon, Fig. 7). Especially Enceladus' water ice spectrum exhibits less opaque material inclusion than any other satellite in the outer Solar System. Therefore it is characterized by the highest geometric albedo of any known airless body in the Solar System (= 1.0; [90Bur2]).

Other ices on outer planet satellites: Triton

Of all icy objects known in the Solar System, Triton, the largest satellite of Neptune, has the most spectrally diverse surface, with four different ices, i.e. N_2, CH_4, CO, CO_2, identified to date [79Cru, 84Cru1, 91Cru, 93Cru, 84Cru2] with N_2 as the dominant surface constituent (Fig. 8). Solid N_2 dominates the surface with most of the CH_4 and probably CO incorporated as a solid solution. Additional compounds, i.e. organic solids, may be within and be deposited on the icy surface.
The extreme seasonal cycle experienced by Triton may cause its surface layers and atmosphere to change through sublimation and re-deposition of volatiles, as well as the alteration of the physical and photometric (see Section 4.2.3.6.1) characteristics of the ices.

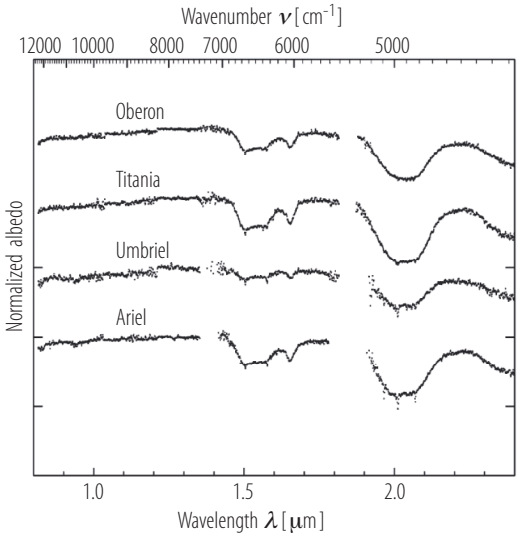

Fig. 7. Example spectra of Uranian satellites. Gaps around 1.4 and 1.85 μm coincide with high atmospheric opacity. The Ariel spectrum is an average of all spectra with subsolar longitudes between 210° and 330°. The Umbriel spectrum is from 2005/09/18 UT and the Titania and Oberon spectra are both from 2005/10/13 UT [06Gru].

In addition to ice(s) outer Solar System satellites surfaces contain a varying amount of a in the visible light dark, mostly spectrally neutral component. Although the dark non-ice material is not fully identified yet, it probably consists of pure carbon, complex organics of various kinds as found in carbonaceous chondrite material [80Cru, 81Cru, 81Soi, 84Bro, 05Cla, 07Cru] and other neutrally colored low albedo materials probably of exogenic origin. Among the many low-albedo satellites, the most striking is Iapetus with its hemispheric dark side centered on the apex of orbital motion, i.e. the leading hemisphere [85Bel].

A considerable amount of hydrated minerals has been identified on Europa which are associated with lineaments and mottled chaotic terrains, regions of most recent disruption [98McC, 99McC] (Fig. 10).

Thus, the hydrated minerals on Europa represent the only example of non-ice material on an outer planet satellite' surface possibly formed by endogenic processes, probably related to a briny ocean below the surface.

Various minor compounds have also been discovered in the surface materials of almost all icy satellites. They are apparently both indigenous and due to radiation processing. CO_2 has been reported first to exist on the Galilean satellites [96Car, 98McC, 00Hib] and more recently also on most of the Saturnian satellites [05Cla, 05Bur, 08Cla]. CO_2 has been found escaping from at least Callisto [99Car].

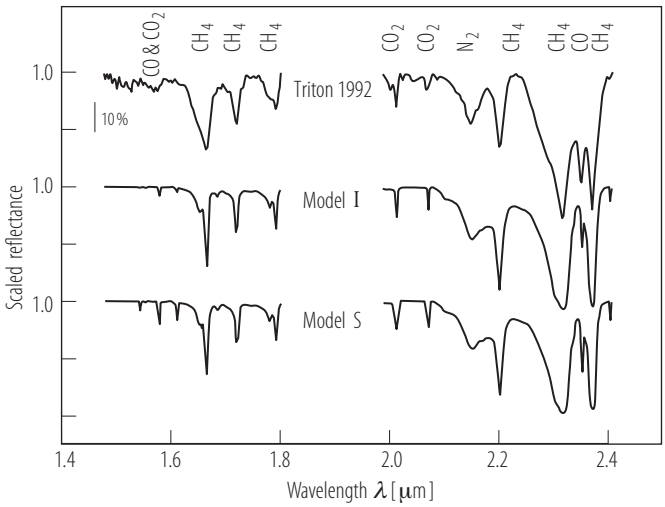

Fig. 8. Observed spectrum of Neptuns' satellite Triton compared to theoretically developed intimate mixtures of relevant ices with 99.75% N_2, 0.10% CO, 0.05% CH_4, and 0.10% CO_2. CO_2 ice is either intimate mixed like the other ice compounds (Model I) or spatially segregated (Model S). For detailed information see [93Cru].

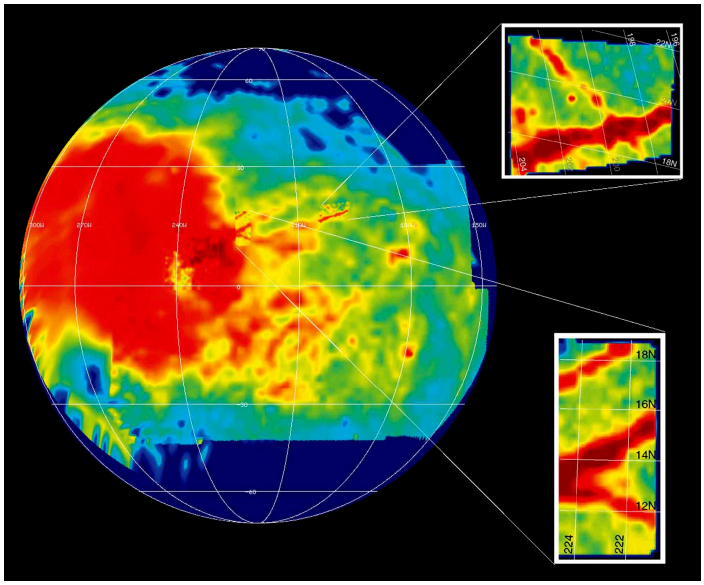

Fig. 9. (see also color-picture part, page 621) Distribution of hydrated minerals on Europa [98McC, 99McC].

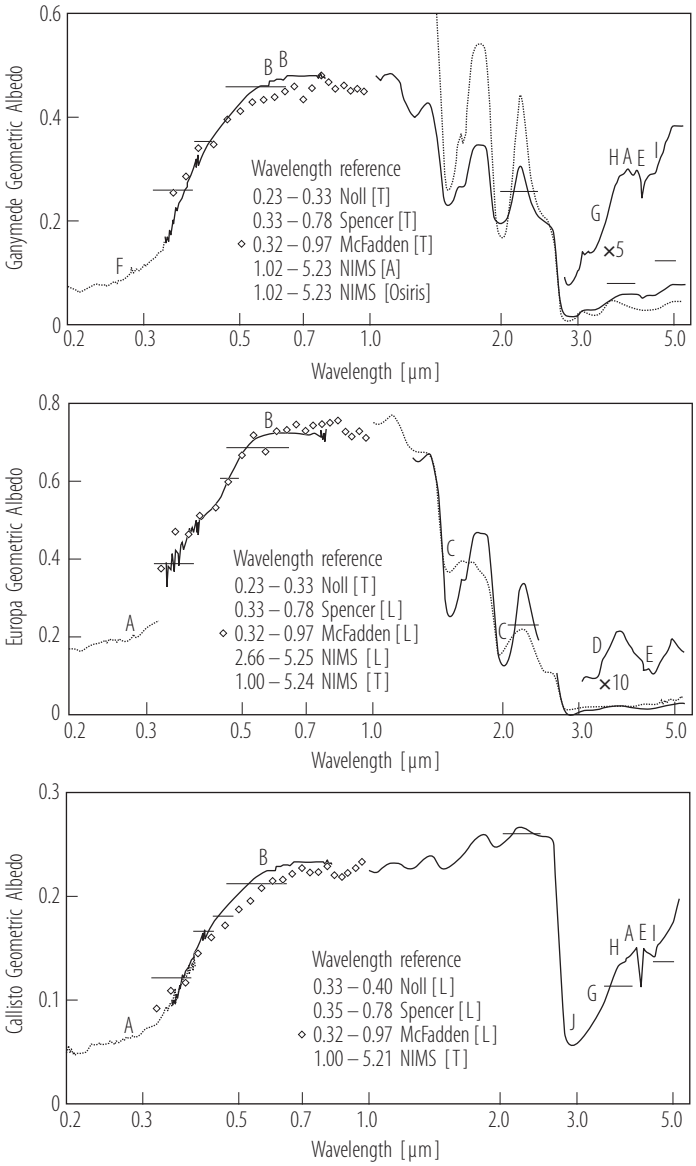

Fig. 6. Reflectance spectra of Europa, Ganymede, and Callisto - Spectral identifications: A = SO_2 gas; B = O_2 or SnO; C = bound H_2O; D = H_2O_2; E = CO_2; F = O_3; G = C-H (?); H = S-H (?); I = C-N (?); J = O-H or bound H_2O. Other features [at 1.04, 1.25, 1.5, and 2 μm] are due to HO_2 frost. References: Noll = [97Nol]; Spencer = [95Spe]; McFadden = [80McF]; NIMS = [98McC]. (L = leading hemisphere; T = trailing hemisphere; J = Jupiter facing hemisphere; A = Anti Jovian hemisphere; Osiris = bright icy crater) [04Spe].

Other constituents were also reported from absorptions in the 3 - 5 μm region in the Jovian system at least for Ganymede and Callisto (SO_2, S-H, C≡N, C-H) [98McC], and throughout the Saturnian system (C≡N, C-H) [05Cla, 07Cru, 08Cla]. However, the near-complete coverage of the outer planets satellites surface by water ice particles, which absorb strongly in this spectral region, allows little radiation to be reflected, and thus signatures of minority minerals are easily hidden.

Nevertheless H_2O_2 was identified by its characteristic absorption at 3.5 μm on all three icy Galilean satellites [99Car] and on Enceladus [07New] and thought to be a product of radiolysis of water ice [00Moo].

An UV absorber concentrated on the trailing side of Europa [98Hen] could be attributed to sulfur delivered to the surface from Io by the Jupiter's magnetosphere. O_3 produced and trapped in the H_2O at least on Ganymede, Dione, and Rhea was identified due to its absorption band at 0.26 μm [97Nol]. O_2 was detected on Ganymede and may be present in the Saturnian system, but it has not been identified yet. Thus the influence of Saturns magnetospheric particles on the composition of the Saturnian satellites appear to be similar to that in the Jupiter system.

4.2.3.6.2.5 X-ray, gamma-ray, and neutron spectroscopy

The interaction of galactic cosmic rays, solar radiation, and the material of a celestial body generates secondary particles: x-rays, gamma-rays, and neutrons. Gamma-ray and x-ray spectroscopy has been used for determining the elemental composition of planetary surfaces [78Ree], [85Sur] by remote sensing if an intervening thick atmosphere is not present. These methods make it possible to determine the content of basic rock-forming (Fe, Ti, Mg, Al, Ca, Si and O) and natural radioactive elements (Th, U, K) by measuring the characteristic gamma-ray line emissions of specific element produced by either nuclear spallation (i.e. neutron inelastic scatter and thermal neutron capture) or radioactive decay reactions, respectively. The secondary neutron field formed in the vicinity of extraterrestrial bodies also carries information about the composition of the planetary regolith. The neutron flux is determined to a large extent by H_2O content and the concentrations of some elements that have anomalous neutron characteristics. The content of H, C, Fe, and elements which have an anomalously large absorption cross section of thermal neutrons e.g. Cl, B, and Li exert the dominating influence on the spatial-energy distribution of neutrons.

This method requires a close spacecraft approach or a lander and therefore was applied especially to Moon and Mars where detailed maps of the distribution and abundance of major elements are available.

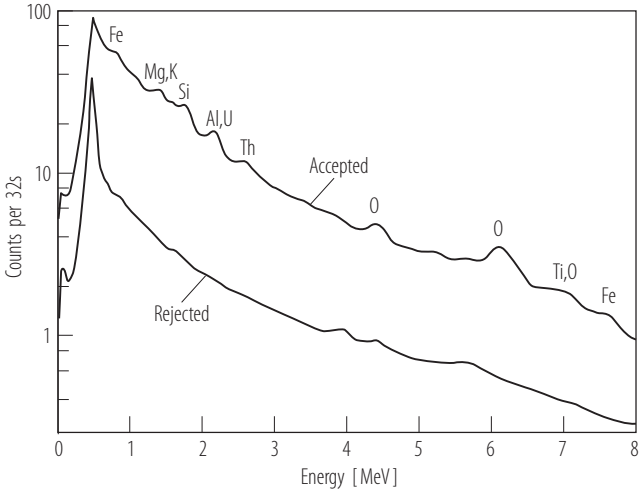

Fig. 10. Accepted and rejected gamma-ray spectra summed up over the entire mapping portion of the mission. Some of the important lines for measuring surface composition are labeled in the accepted spectra. These include the radioactive elements K, U, and Th (1.46, 2.22, and 2.61 MeV); other strong lines include Fe (0.846 and 7.64 MeV), Mg (1.38 MeV), Si (1.78 MeV), Al (2.22 MeV), O (4.44, 6.13, 6.92 MeV), and Ti (6.76 MeV) [04Law].

Table 8. Distribution of ices in the Solar System. NOTES: HC = hydrocarbon of unknown composition; XCN = contribution from a chemical species with a C-N triple bond; SH = contribution from a chemical species with an S-H single bond (adapted from [07Hud]).

Planetary object	Ices
Earth	**H_2O**
Mars	**H_2O**, CO_2
Jupiter	
Io	SO_2, SO_3, H_2S?, H_2O?
Europa	**H_2O**, SO_2, SH, CO_2, O_2, HC, XCN, H_2O_2, H_2SO_4, carbonate salt, hydrous sulphate
Ganymede	**H_2O**, SO_2, SH, CO_2, HC, XCN, O_2, O_3, hydrated and hydroxylated minerals
Callisto	**H_2O**, SO_2, SH, CO_2, HC, XCN, hydrated and hydroxylated minerals
Saturn	
Mimas	**H_2O**
Enceladus	**H_2O**
Tethys	**H_2O**

Planetary object	Ices
Dione	**H_2O**, C, HC, O_3
Rhea	**H_2O**, HC?, O_3
Hyperion	**H_2O,** CO_2, CN
Iapetus	**H_2O**, C, HC, CO_2, CN, H_2S?
Phoebe	**H_2O**, CO_2, CN, CH
Titan	H_2O, $C_2(CN)_2$
Rings	**H_2O**, HC?
Uranus	
Miranda	**H_2O**, NH_3 (NH_3 hydrate?), hydroxylated silicates
Ariel	**H_2O**, CO_2, OH?
Umbriel	**H_2O**
Titania	**H_2O**, C, HC, OH?
Oberon	**H_2O**, C, HC, OH?
Neptune	
Triton	N_2, CH_4, CO, CO_2, H_2O

Table 9. Elemental composition of Mars [93Sur] and Moon [78Ree] measured using orbital gamma-ray spectroscopy. *Gamma-rays were produced by the following processes: N - decay of natural activity, I - neutron inelastic scatter, C - neutron capture.

			Mars			Moon	Reaction type*
Element	Phobos 2	Mars 5	Viking 1	Viking 2	GRS	AGRS	
O	48 ± 5	44 ± 5	50.1 ± 4.3	50.4		43.5	I
Mg	6 ± 3		5.0 ± 2.5				I
Al	5 ± 2	5 ± 2	3.0 ± 0.9			11	I/C
Si	19 ± 4	14 ± 3	20.9 ± 2.5	20	18.5 - 21.5	20	I
K	0.3 ± 0.1	0.3 ± 0.1	0.25	0.25		1200 µg/g	N
Ca	6 ± 3		4.0 ± 0.8	3.6		10	C
Ti	1 ± 0.5		0.51 ± 0.2	0.61		1.4	C
Fe	9 ± 3	14 ± 4	12.7 ± 2.0	14.2		9	C/I
Th	$(1.9 \pm 0.6) \times 10^{-4}$	$(2.1 \pm 0.5) \times 10^{-4}$				1.9 µg/g	N
U	$(0.5 \pm 0.1) \times 10^{-4}$	$(0.6 \pm 0.1) \times 10^{-4}$				0.5 µg/g	N

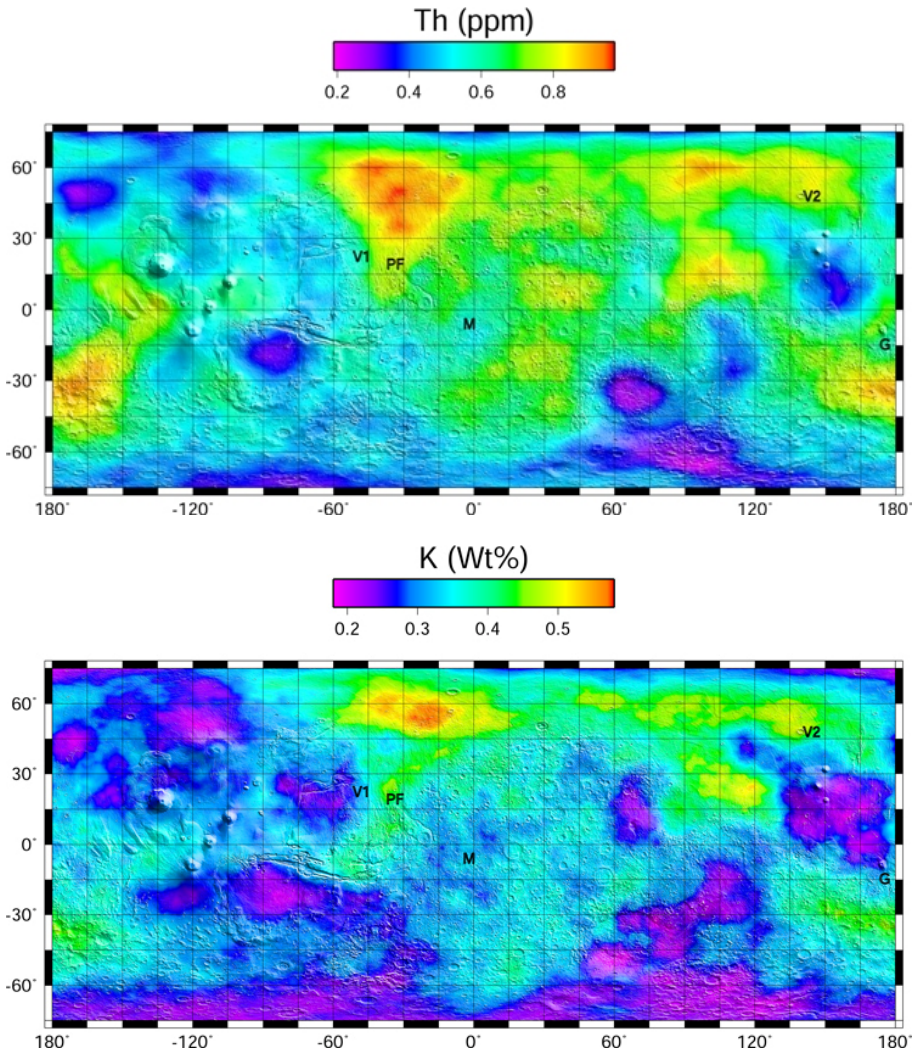

Fig. 11. (see also color-picture part, page 622) Maps of the distribution of K and Th on Mars, as measured by the Mars Odyssey gamma-ray spectrometer. Data have been smoothed using a 10 by 10 pixel boxcar filter. The data are displayed over a shaded relief map of Mars, with mission landing sites indicated: V1 and V2, Viking 1 and 2; PF, Pathfinder; M, Opportunity in Meridiani Planum; G, Spirit in Gusev Crater [06Tay].

Table 10. Comparison of K, Th, and K/Th in Mars, Earth, asteroid Vesta, the Moon, and carbonaceous chondrites

	K [ppm]	Th [ppm]	K/Th	References
Mars (average crust)	3300	0.62	5300	[06Tay]
Mars bulk silicate-WD	305	0.056	5450	[84Dre], [88Wän], [94Wän]
Mars bulk silicate-L	920	0.056	16,400	[97Lod]
Mars bulk silicate-MA	77	0.125	620	[79Mor]
Earth continental crust	11,000	4.2	2600	[85Tay]
Earth bulk silicate	230	0.079	2900	[85Tay], [79Jag], [95McD]
Vesta (HED meteorites)	420	0.40	1050	[98Kit], [93Mit]
Moon (high-K KREEP)	8000	22	360	[79War], [89War]
CI chondrites	550	0.029	19,000	[95McD]

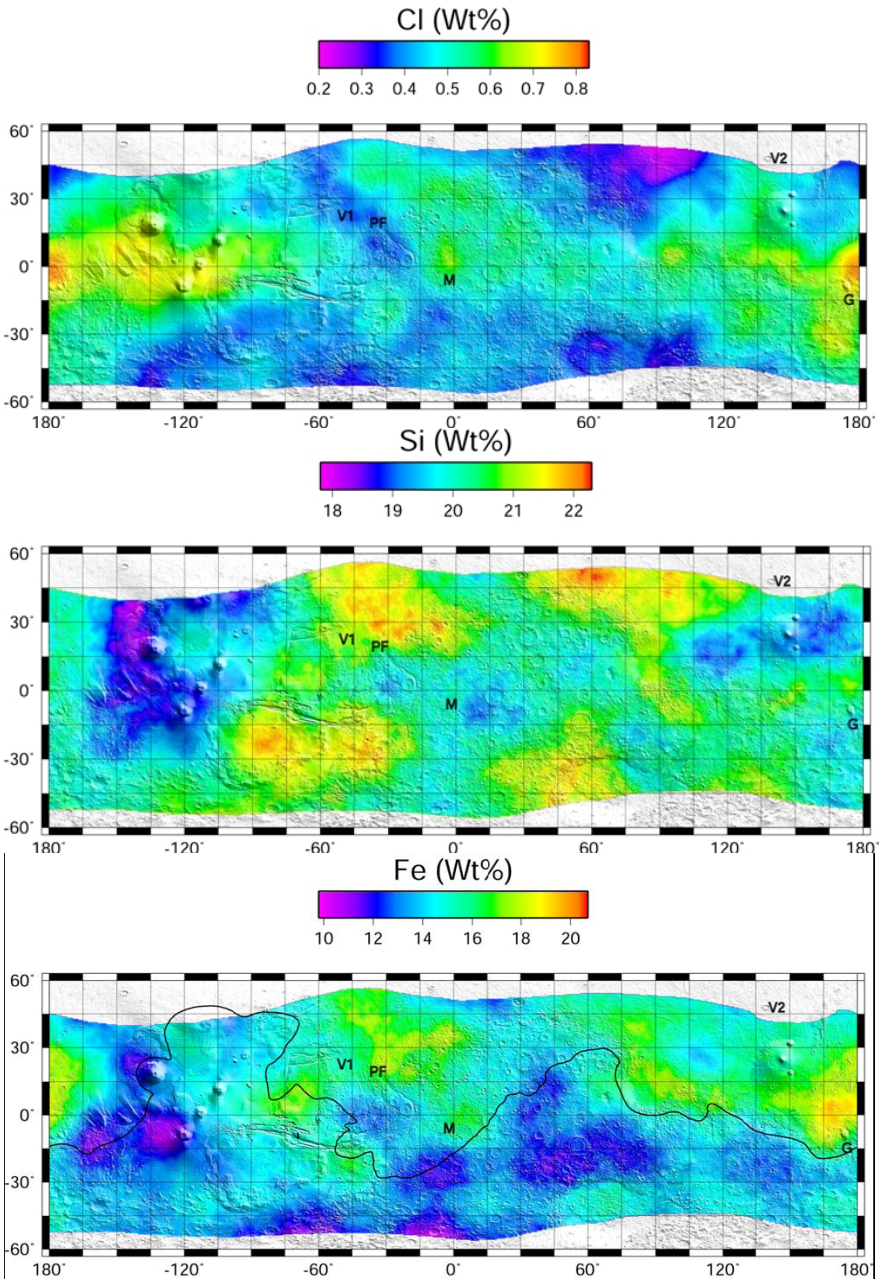

Fig 12. (see also color-picture part, page 623) Map of the distribution of Cl, Si, and Fe on Mars as measured by the Mars Odyssey gamma-ray spectrometer. Data have been smoothed using a 10 by 10 pixel boxcar filter. The mapped area encompasses only hat portion of Mars in which H content does not dominate. The data are displayed over a shaded relief map of Mars, with mission landing sites indicated: V1 and V2, Viking 1 and 2; PF, Pathfinder; M, Opportunity in Meridiani Planum; G, Spirit in Gusev Crater. The black line represents the 0-km contour, a reasonable separation between highlands and lowlands [06Tay].

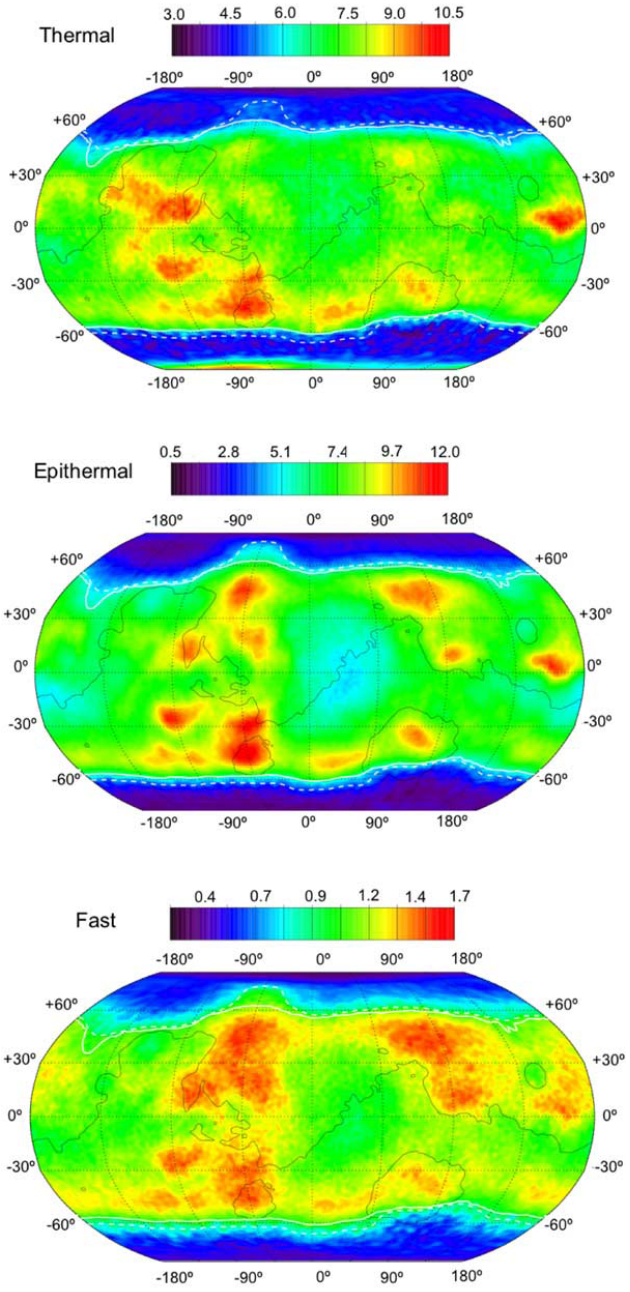

Fig. 13. (see color-picture part, page 624) Thermal, epithermal, and fast neutron CO_2 frost-free maps of Mars. Data north of the northern white dashed wavy line were measured after the northern summer solstice ($100 < Ls < 151$), and data south of the southern dashed wavy line were measured during the late summer in the south ($329 < Ls < 1.7$). The 0-km elevation contour (black line) is included for reference. The solid white lines separate the poleward regions having water abundances larger than about 11% by mass from those at near equatorial latitudes that have abundances that are less than 11% [02Fel].

4.2.3.6.3 References for 4.2.3.6

53Joh Johnson, H.L., Morgan, W.W.: Astrophysical Journal (1953) 117, 313.
60Sin Sinton, W.H., Strong, J.: Astrophys. J. **131** (1960), 459.
61Har Harris, D.L.: In: Kuiper, G.P., Middlehurst, B.M., editors, Photometry and colorimetry of planets and satellites, Planets and Satellites. Univ. of Chicago Press, Chicago, 1961, 272-342.
70Bur Burns, R.: Mineralogical Applications of Crystal Field Theory, Cambridge University Press, Cambridge, 1970, 224.
71Neu Neugebauer, G., et al.: Astron. J. **76** (1971) 719.
72Han Hanel, R., et al.: Icarus **17** (1972) 428.
73Lan Lane, A.P., Irvine, W.M.: Astron. J. **78** (1973) 267.
75Ada Adams, J.B.: In: Infrared and Raman Spectroscopy of Lunar and Terrestrial Minerals, Academic Press, New York, 94-116, 1975.
75Str Strom, R., et al.: J. Geophys. Res. **80** (1975) 2478.
76Ast Astronomical Quantities, third edition, Uni. of London (1976), 144.
76Fin Fink, U. et al.: Astrophysical Journal **207** (1976), L63.
76Zel Zellner, B., Gradie, J.: Icarus **81** (1976) 262.
77Cam Campbell, D.B., et al.: Science **196** (1977) 650.
77Mor Morrison, D.: In: Burns, J.A., editor, Planetary Satellites, Uni. of Arizona Press, Tucson, 1977, 269 - 301.
78Bow Bowell, E., et al.: Icarus **35** (1978) 313.
78Cam Campbell, D.B., et al.: Icarus **134** (1978), 292.
78Nel Nelson, R.M., Hapke, B.W.: Icarus **36** (1978) 304.
78Ree Reedy, R.C., Planetary gamma-ray spectroscopy, Proc. LunarPlanet. Sci. Conf. 9^{th} (1978), 2961.
79Bow Bowell, E., Lumme, K.: In: T. Gehrels, editor, Asteroids, Uni. of Arizona Press, Tucson, 132 - 169, 1979.
79Cru Cruikshank, D.P.: Icarus **41** (1980) 246.
79Cru Cruikshank, D. P., Silvaggio, P. M.: Astrophys. J. **233** (1979) 1016.
79Jag Jagoutz, E., et al.: The abundances of major, minor, and trace elements in the Earth's mantle as derived from primitive ultramafic nodules, Proc. Lunar Planet. Sci. Conf., 10th, (1979), 2031.
79Kie Kieffer, H.H.: J. Geophys. Res. **84** (1979) 8263.
79Mor Morgan, J.W., Anders, E: Geochim. Cosmochim. Acta **43** (1979) 1601.
79Sei Seiff, A., et al.: Science **205** (1979) 46.
79War Warren, P.H., Wasson, J.T.: Rev. Geophys. **17** (1989) 73.
79Zel Asteroid taxonomy and the distribution of compositional types, in: Asteroids (T. Gehrels, Ed.) Uni. of Arizona Press, Tucson (1979), 783 - 806.
80Cam Campbell, D.B., Burns, B.A.: J. Geophys. Res. **98** (1980) 15003.
80Cru Cruikshank, D.P.: Icarus **41** (1980) 246.
80Deg Degewij, J, et al.: Icarus **44** (1980) 520.
80Hun Hunt, G.R.: In: B. Siegal and A. Gillespie, editors, Remote Sensing in Geology (1980) 5-45.
80McF McFadden, L.A., et al.: Icarus **44** (1980) 410.
81Cru Cruikshank D.P., Brown: Icarus **45** (1981) 607.
81Hap Hapke, B.W.: J. Geophys. Res. **86** (1981) 3039.
81Lum Lumme, K., Bowell, E.: Astron. J. **86** (1981) 1694.
76Ast Astronomical Quantities, third edition, Uni. of London (1976), 144.
81Soi Soiffer, B.T., et al.: Icarus **45** (1981) 612.
82Bro Brown, R.H.: The satellites of Uranus – spectrophotometric and radiometric studies of their surface properties and diameters. Ph.D. Thesis, Univ. of Hawaii, Honolulu (1982).
82Fan Fanale, F.P., et al.: In: D. Morrison, editor, Satellites of Jupiter, Univ. of Arizona Press, Tucson, 1982, 756 - 781.
82Han Hanel, R., et al.: Science **233** (1982) 544.
82Ost Ostro, S.J.: In: D. Morrison, editor, Satellites of Jupiter (1982), 213-236.
84Bro Brown, R.H., Clark, R.N.: Icarus **58** (1984) 288.
84Cru1 Cruikshank D.P., et al.: Icarus **58** (1984) 293.

84Cru2 Cruikshank D.P., Apt, J.: Icarus **56** (1984) 306.
84deP de Pater, I., et al.: Icarus **57** (1984) 93.
84Dre Dreibus, G., and Wänke, H.: Accretion of the Earth and the inner planets, Proc. Int. Geol. Conf. (1984) 27th (11), 1 - 20.
85Bel Bell, J. F., et al.: Icarus **61** (1985) 192.
85Bur Buratti, B. J.: Icarus **61** (1985) 208.
85Gad Gaddis, L.R., et al.: Icarus **61** (1985) 461.
85Sur Surkov Y.A., et al.: Astronom. Vestnik **19** (1985) 275 (in Russian).
85Tay Taylor, S.R., and McLennan, S.M.: The Continental Crust: Its Composition and Evolution, Blackwell Sci., Malden, Mass (1985), 312.
86Cla Clark, R.N., et al.: In: Satellites, edited by J. Burns and M.S. Matthews, Univ. of Arizona Press (1986), Tucson, 461-486.
86Han Hanel, R. et al.: Science **233** (1986) 70.
86Nel Nelson, R.M., Smythe, W.D.: Icarus **66** (1986) 181.
86Pie Pieters, C.M.: Rev. Geophys. **924** (1986) 557.
86Sim Simonelli, D.P., Veverka, J.: Icarus **68** (1986) 503.
86Vev Veverka, J., et al.: In: Burns, J., Matthews, M.S., editors, Satellites, Univ. of Ariz. Press, Tucson (1986), 342-402.
86Vil Vilas, F., et al.: Icarus **59** (1984) 60.
87Cru Cruikshank, D.P.: Adv. Space Res. **7(5)** (1987) 109.
87Hel Helfenstein, P., Veverka, J.: Icarus **72** (1987) 342.
87Spe Spencer, J.R.: Icarus **70** (1987) 99.
87Tho Thompson, T.W.: Earth Moon Planets **37** (1987) 59.
88Bur Buratti, B.J., et al.: Nature **333** (1988a) 148.
88Cla Clark, P.E., et al.: In: Vilas F., et al., editors, Mercury, Univ. of Arizona Press, Tucson, 1988, 77-100.
88Hel Helfenstein, P., et al.: Icarus, **74** (1988) 231.
88Vev Veverka, J., et al.: In: Vilas, F., et al., editors, Mercury, Univ. of Ariz. Press, Tucson, 1988, 37-58.
88Vil Vilas, F.: In: Vilas, F., et al., editors, Mercury, Univ. of Arizona Press, Tucson, 1988, pp. 59 - 76.
88Wän Wänke, H., Dreibus, G.: Chemical composition and accretion history of the terrestrial planets, Philos. Trans. R. Soc. London (1988), Ser. A, 325, 545 - 557.
89Con Conrath, B., et al.: Science **246** (1989) 1454.
89Nas Nash, D.B., Howel, R.R.: Science **244** (1989) 454.
89Ver Verbiscer, A.J., Veverka, J.: Icarus **82** (1989) 336.
89War Warren, P.H. (1989), KREEP: Major element diversity, trace-element uniformity (almost), in Workshop on Moon in Transition: Apollo 14, KREEP, and Evolved Lunar Rocks, edited by G.J. Taylor and P.H. Warren, Tech. Rep. Lunar and Planet. Inst., Houston, Tex. (1989) 89 - 03, 149 - 153.
90Bur1 Buratti. B.J., et al.: Icarus **84** (1990) 203.
90Bur2 Buratti, B.J., et al.: Icarus **87** (1990) 339.
90Hil Hillier, J., et al.: Science, **250** (1990) 419.
90Muh Muhleman, D.O., et al.: Science **248** (1990) 975.
90Pol Pollack, J.B., et al.: J. Geophys. Res. **95 (B9)** (1990) 14,595 - 14,627.
90Sal Salama, F., et al.: Icarus **83** (1990) 66.
91Bur Buratti, B.J.: Icarus **92** (1991) 312.
91Cru Cruikshank D.P., Allamandolat, L.J.: Icarus **9** (1991) 345.
91Dom Domingue, D.L., et al.: Icarus, **90** (1991) 30.
91Mos Moses J.I., Nash, D.B.: Icarus **89** (1991) 277.
92Har1 Harmon, J.K., Slade, M.A.: Science **258** (1992) 640.
92Har2 Harmon, J.K.,et al.: Icarus **98** (1992) 240.
92Ost Ostro, S.J., et al.: J. Geophys. Res. **97** (1992) 18227.
92Sla Slade, M.A., et al.: Science **258** (1992) 635.

93Ast Astronomical Almanac, http://asa.usno.navy.mil/SecF/2008/Satellite_photo_data.txt, U.S. Nautical Observatory, Publication Washington (1993).
93Bur Burns, R.G.: In: Pieters, C.M., Englert, A.J. (Eds.), Remote Geochemical Analysis: Elemental and Mineralogical Composition. Cambridge Univ. Press (1993), Cambridge, 3 - 29.
93But Butler, B.J., et al.: J. Geophys. Res. **98** (1993) 15003.
93Cru Brown, R. H., Clark, R. N.: Icarus **58** (1984) 288.
93Hil Hillier, J.: Voyager Photometry of Triton, PhD. Thesis, Cornell University (1993).
93Mit Mittelfeldt, D., Lindstrom, M.: Proc. Natl. Inst. Polar Res. Symp. Antarct. Meteorites **6** (1993) 268.
93Sal Salisbury, J.W.: In: C.M. Pieters, P.A.J. Englert, editors, Remote Geochemical Analysis: Elemental and Mineralogical Composition, Cambridge University Press (1993), Cambridge, 79-98.
93Sur Surkov, Yu.A., Moskaleva, L.P., Kharyukova, V.P., Manvelyan, O.S., and Golovin, A.: In: C. M. Pieters, and P.A.J. Englert (Eds.) Remote Geochemical Analysis: Elemental and Mineralogical Composition, Cambridge University Press (1993), Cambridge, 413-425.
93Van Vane, G., et al.: In: C. M. Pieters, and P.A.J. Englert (Eds.) Remote Geochemical Analysis: Elemental and Mineralogical Composition, Cambridge University Press (1993), Cambridge, 121-143.
94Kar Karkoschka, E.: Icarus **111** (1994) 174.
94Spr Sprague, A.L., et al.: Icarus **109** (1994) 156.
94Wän Wänke, H., Dreibus, G.: Philos. Trans. R. Soc. London **Ser. A, 349** (1994) 285.
95Bur Buratti, B.J.: JGR **100 E9** (1995) 19061.
95Kha Khana, R.K., et al.: Icarus **115** (1995) 250.
95McD McDonough, W.F., Sun, S.-s.: Chem. Geol. **120** (1995) 223.
95Spe Spencer, J.R., et al.: J. Geophys. Res. **100** (1995) 19049.
96Car Carlson, R., et al.: Science **274** (1996) 385.
96Mur Murchie, S., Erard, S.: Icarus **123** (1996) 63.
96Ort Orton, G.S., et al.: Science **274** (1996) 389.
97Ble Blewett, D.T., et al.: Icarus **129** (1997) 217.
97Cam Campbell, B.A., et al.: J. Geophys. Res. **102** (1997) 19,307.
97Car Carlson, R.W., et al.: Geophys. Res. Lett. **24** (1997) 2479.
97Dom Domingue, D., Verbiscer A.: Icarus **128** (1997) 49.
97Lod Lodders, K., Fegley Jr., B.: Icarus **126** (1997) 373.
97Nol Noll, K.S., et al.: Nature **388** (1997) 45.
97Vid Vidal, R.A., et al.: Science **276** (1997) 1839.
98Eme Emery, J.P., et al.: Icarus **136** (1998) 104.
98Hen Hendrix, A.R., et al.: Icarus **135** (1998) 79.
98Kit Kitts, K., Lodders, K.: Meteorit. Planet. Sci. **33** (1998) A197.
98McC McCord, T.B., et al.: J. Geophys. Res. **103** (1998) 8603.
98Nas Nash, D.B., Betts, B.H.: In: B. Schmitt, C. De Bergh, and M. Festou (Eds.) Solar System Ices, Astrophys. Space Sci. Lib., Kluwer Academic, Dordrecht (1998), 607 - 637.
98Sim Simonelli, D.P., et al.: Icarus **131** (1998) 52.
98Spr Sprague, A.L., Roush, T.L.: Icarus **133** (1998) 174.
99Car Carlson, R.W., et al.: Science **283** (1999) 2062.
99Har Hartmann, W.K., Moons & Planets, Fourth Edition, Wadsworth Publishing Company (1999), 428.
99McC McCord, T.B., et al.: J. Geophys. Res. **104 E5** (1999) 11827.
99Spe Spencer, J.R., et al.: Science **288** (1999) 1198.
99Vas Vasavada, A.R., et al.: Icarus **141** (1999) 179.
00Hib Hibbitts, C.A., et al.: J. Geophys. Res. **105 E09** (2000) 22,541.
00Kie Kieffer, H.H., et al.: J. Geophys. Res. **105 E04** (2000) 9653.
00Mar Digital elevation models of the Moon from Earth-based radar interferometry. IEEE Geosci. Rem. Sens. **38** (2000) 1122.
00Mil Mills, F.P., Brown, M.E.: J. Geophys. Res. **105 E6** (2000) 15,051.

00Moo Moore, M.H., Hudson, R.L.:Icarus **145** (2000) 282.
01Bla Black, G.J., et al.: Icarus **151** (2001) 160.
01Coo Cooper, B., et al.: J. Geophys. Res. **106 (12)** (2001) 32,803.
01Dou Douté, S., et al.: Icarus **149** (2001) 107.
01Kie Kieffer, H.H., Titus, T.N.: Icarus **154** (2001) 162.
02Ban Bandfield, J.L., et al.: Science **287** (2000) 1626.
02Spr Sprague, A.L., et al.: Meteorit. Planet. Sci. **37** (2002) 1255.
02War Warell, J.: Icarus **156** (2002) 303.
03Gad Gaddis, L.R., et al.: Compositional analyses of lunar pyroclastic deposits. Icarus **161** (2003) 262.
03Cam Campbell, D.B., et al.: Science **302** (2003) 431.
03Sch Schmitt, B., Rodriguez, S.: J. Geophys. Res. **108 E9** (2003) 5104.
04Spe Spencer, J.R., et al.: In: Jupiter – The Planet, Satellites and Magnetosphere (F. Bagenal, T. Dowling, W. McKinnon, Eds.), Cambridge Uni. Press, Cambridge (2004) 689 - 699.
04Law Lawrence, D.J., et al.: J. Geophys. Res. **109** (2004) E07S05.
04Moo Moore, J.M., et al.: Callisto, Jupiter – The Planet, Satellites and Magnetosphere (Ed. F. Bagenal, T. E. Dowling, W. B. McKinnon), Cambridge Univ. Press (2004) 397-426.
05Bib Bibring, J.P., et al.: Science **307** (2005) 1576.
05Bur Buratti, B.J., et al.: Astrophys. J **622** (2005) L149.
05Chr Christensen, P.R., et al.: Nature (2005) 436, doi:10.1038/nature03639.
05Cla Clark, R.N., et al.: Nature (2005).
05Fla Flaser, F.M. et al.: Science **307** (2005) 1247.
05Gen Gendrin, A., et al.: Science **307** (2005) 1587.
05Ghe Ghent, R.R., et al.: J. Geophys. Res. (2005) 110, doi: 10.1029/2004JE002366.
05Cam Campbell, B.A., Hawke, B.R.: J. Geophys. Res. (2005), doi:10.1029/2005JE002425.
05Lan1 Langevin, Y., et al.: Science **307** (2005a) 1581.
05Lan2 Langevin, Y., et al.: Science **307** (2005b) 1584.
05Mus Mustard, J.F., et al.: Science **307** (2005) 1594.
05Pou Poulet, F., et al.: Nature **438** (2005) 623.
05Yen Yen, A. S., et al.: Nature **436** (2005) 49.
06Cam Campbell, B.A., Campbell, D.A.: Icarus **180** (2006) 1.
06Gru W.M. Grundy, et al.: Icarus **184** (2006) 543.
06Har Harmon, J.K., et al.: Icarus (2006) **187** 374.
06Jac Jacobson, R.A.: JPL Solar System Dynamics, http://ssd/jpl.nasa.gov/?sat_elem (2006).
06Nic Nicholson, P.D.: In: The Observer's Handbook 2006, Rajiv Gupta (Eds.), University of Toronto Press, Toronto (2005), 20 - 26.
06Ost Ostro, S.J., et al.: Icarus **183** (2006), 479.
06She Sheppard, S.S., at "The Giant Planet Satellite Page", http://www.ifa.hawaii.edu/~sheppard /satellites/ (2006).
06Spe Spencer, J.R., et al.: Science **311(5766)** (2006) 1401-1405. DOI: 10.1126/science.1121661
06Tay Taylor, G.J., et al.: J. of Geophys. Res. **111** (2006), E03S10; 2006 [printed 112(E3), 2007].
06War Warell, J., et al.: Icarus **180** (2006) 281.
07Bla Black, G.J., et al.: Icarus **191** (2007) 702.
07Bus Busch, M.W., et al.: Icarus **186** (2007) 581.
07Cru Cruikshank, D.P., et al.: Icarus (2007), doi: 10.1016/j.icarus.2007.04.036.
07For F., Forget, F., et al.: J. Geophys. Res. **112** (2007) E08S12.
07Hud Hudson 2007 The Cosmic Ice Laboratory http://www-691.gsfc.nasa.gov/cosmic.ice.lab/
07Lan Langevin, Y., et al.: J. Geophys. Res. **112** (2007) E08S12.
07Mit Mitri, G.: Icarus **186** (2007) 385.
07New Newman, S.F., et al.: The Astrophysical Journal **670** (2007) L143.
07Pel Pelkey, S.M., et al.: J. Geophys. Res. **112** (2007) E08S14.
07Wye Wye, L.C., et al.: Icarus **188** (2007) 367.
08Cla Clark, R.N., et al.: Icarus **193** (2008).